Pol. J. Environ. Stud. Vol. 32, No. 2 (2023), 1447-1458
DOI: *10.15244/pjoes/156426* ONLINE PUBLICATION DATE: 2023-01-13

Original Research

Joint Toxic Action and Metabolic Mechanisms of Graphene Nanomaterial Mixtures in *Microcystis Aeruginosa*

Jieyu Zhao, Yajie Liang*, Li Jin, Huan Zhang, Benying Shi, Xiwang Tang

Department of Environmental Engineering, Hebei University of Environmental Engineering, Qinhuangdao 066102, China

Received: 30 August 2022
Accepted: 10 November 2022

Abstract

Graphene family nanomaterials are used in a broad range of applications. These materials have been released into the aquatic system where they can have toxicological effects in non-target organisms. Although several studies have investigated their toxicity, there is little information on the toxicity and mechanisms of graphene nanomaterial mixtures in *Microcystis aeruginosa*. This study investigated the toxicities of individual and binary mixtures of graphene family nanomaterials (graphene oxide (GO), GO quantum dots (GOQD), and carboxylic acid-functionalized single-walled carbon nanotubes (C-SWCNT)) in *M. aeruginosa*. The toxicological interaction profiles of the mixture rays were also examined. The results showed that the three types of nanoparticles and their binary mixture rays had significant inhibitory and hormetic effects in *M. aeruginosa*. Metabolomics analysis showed that the nanomaterials had different toxicity mechanisms. Amino acid metabolism was sensitive to GO exposure, while C-SWCNT and GOQD exposure led to a sharp decline in sugars and an increase in fatty acids, respectively. The toxicological interactions in the binary GO and GOQD mixtures were different from that of the GO and C-SWCNT mixtures. These findings increase our understanding of the nanotoxicity and toxicity mechanisms of GO, C-SWCNT, and GOQD and will aid in the risk assessment of nanomaterials in aquatic environments. Amino acids, sugars, and fatty acids can be used as indicators of the corresponding biological responses to these nanomaterials.

Keywords: graphene oxide, quantum dot, carbon nanotubes, joint toxic action, direct equipartition ray design, metabolomics

*e-mail: liangyajie12@126.com

Introduction

Graphene oxide (GO) has useful mechanical and hydrophilic properties and is highly flexible and ductile. Thus, it has been extensively applied in various fields, including environmental protection [1], medicine [2], biology [2], and chemistry [3]. The increasing use of graphene nanomaterials has led to their inevitable release into the aqueous environment and poses an ecological risk. The size and shape of nanomaterials play a major role in their biocompatibility and are closely related to the toxicity of these materials [4]. For example, GO is 0.5-5 μm, GO quantum dots (GOQD) have a lateral dimension of approximately 20-50 nm, and carboxylic acid-functionalized single-walled carbon nanotubes (C-SWCNT) are 1-2 nm. Furthermore, toxic pollutants often coexist in the environment. The combined toxicity of graphene-family nanomaterials has been unclear. Therefore, in addition to assessing the toxicity of these pollutants individually, it is necessary to investigate the joint toxic action of graphene-related materials and their corresponding toxicity mechanisms.

The concentration addition (CA) model and the independent action (IA) model have been widely used to investigate the combined effects of environmental contaminants [5, 6]. These two reference models are applicable in different situations. The CA model is assumed to apply to pollutants with similar modes of toxicity, while the IA model is employed to evaluate the joint action of a mixture that contains components with independent modes of action. A new top-to-down method based on CA and IA models was evaluated, which effectively eliminated the effect of cosolvents [7]. The IA model is more appropriate for components that have a hormetic effect. The joint toxic effects of three halogenated organic pollutants were investigated using the IA model. This model is often used to evaluate the combined toxic effect based on different modes of toxicity, particularly the hormetic effect [8].

Microcystis aeruginosa (*M. aeruginosa*) is a bacteria that plays a large role in harmful freshwater algal blooms [9, 10]. For this reason, it has often been used as model organism for evaluating the toxic effects of pollutants such as nanoparticles, antibiotics, and metals [11]. Previous studies have suggested that many types of nanoparticles can induce hormetic responses in *M. aeruginosa* [12]. Hormesis typically shows a biphasic dose-response curve and is not included to evaluate the toxic effects of pollutants in ecological risk assessment [13, 14]. However, there has been little focus on the potential hormetic effects of nanoparticle exposure, and the underlying mechanisms of nanoparticle toxicity remain unclear. The potential hormetic effects of pollutants can contribute to algal blooms, which can degrade the health of the aqueous environment.

Hormetic effects usually involve subtle changes [15]. The common toxicological end points of nanomaterial exposure, such as inhibition of alga growth and changes in biological parameters related to oxidative stress, are difficult to differentiate from natural variability [16]. Metabolomics can be used to precisely identify phenotypic characteristics and provides a snapshot of the nutrient status, abiotic and biotic stress [17, 18], and growth conditions of an organism [19, 20]. In the present study, direct equipartition ray design, an IA prediction model, and *M. aeruginosa* metabolic profiling were employed to explore the specific toxic effects of GO, C-SWCNT, and GOQD and their underlying toxicity mechanisms.

Experimental

Chemicals and Organism

The three graphene family nanomaterials used in this study (GO, GOQD, and C-SWCNT) were purchased from Jiangsu Xianfeng Nanomaterials Technology Co., Ltd. (China). Their physical properties are provided in Table 1. Stock solutions of each material were prepared at their maximum solubility in Milli-Q water and stored at 4ºC. The nanomaterials used to make the stock solutions were of analytical grade. *M. aeruginosa* FACHB-469 (nontoxic strain) was purchased from the Institute of Hydrobiology, Chinese Academy of Sciences (Wuhan, China).

Toxicity Tests

M. aeruginosa was cultured to the exponential phase and then added to sterile 300 mL Erlenmeyer flasks containing standard BG-11 culture medium and different concentrations of graphene family nanomaterials, alone or in binary mixtures. Each flask had a cell concentration of 5.0×10^5 cells/mL and a total volume of 150 mL. Control groups containing no nanomaterial were also established. All of the samples

Table 1. Physical properties of the three nanomaterials.

Nanomaterials	Abbr	Purity	Size
GO quantum dots	GOQD	-	<15 nm
Graphene oxide	GO	>99%	500-5000 nm
Carboxylic acid-functionalized single-walled carbon nanotubes	C-SWCNT	>90%	1-2 nm

were cultured for 7 d at 25ºC under a light intensity of 2500 Lux with a 12 h bright: 12 h dark cycle and shaken three times per day. After culturing, the cell absorbance was determined by an enzyme-labeling instrument. The inhibitory rate was calculated as follows:

$$I_i=(1-\frac{A_i}{A_0})\times 100\%$$

where I_i is the inhibitory rate of the nanomaterial at concentration *i* towards the algae, A_i is the absorbance after culturing the algae with the nanomaterial for 72 h or 7 d, and A_0 is the absorbance of the control group. The dose-response relationship between the nanomaterial and the algae was plotted using the nanomaterial concentration and the corresponding inhibitory rate.

Nanomaterial Mixture Design

The three graphene family nanomaterials were grouped into two binary mixture systems (GO-C-SWCNT and GO-GOQD). To assess the nature of the toxicity of these mixtures at different concentrations of the components, mixture rays with different mixture ratios were established using the direct equipartition ray design (EquRay) procedure [21, 22] for a total of six rays (denoted as GO-C-SWCNT-R1, GO-C-SWCNT-R2, GO-C-SWCNT-R3, GO-GOQD-R1, GO-GOQD-R2, and GO-GOQD-R3). The mixture ratios ($p_{i,j}$) [23] of the two components in the six mixture rays are listed in Table 2. The mixture ratio is the ratio of the concentration of the *j* th component in the *i* th ray to the total concentration of the ray.

Concentration-Response Curve Fitting and Toxicological Interaction

Concentration-response curves (CRCs) were fitted using an Origin software function [21]. The 95% observation-based confidence intervals (OCIs) of the fitted CRCs were also calculated [24]. The root mean square error (RMSE) and coefficient of determination (R) were used to assess the curve fitting performance. The IA model can be used to assess toxicological interactions because it is suitable for predicting combined toxicity, especially there is a hormetic effect in at least one component. The total lethality of the mixture can be calculated as follows:

$$E(C_{mix})=1-\prod_{i=1}^{n}(1-E(c_i))$$

where n is the number of components in the mixture system, C_{mix} is the total concentration of the mixture, $E(C_{mix})$ is the total lethality of the mixture, and $E(c_i)$ is the lethality from the *i* th component with concentration c_i. The joint toxic effect can be assessed by comparing the experimental results of the mixture ray and the IA model results. If the combined toxicity calculated by the IA model is larger than the upper OCI, the joint toxic action is considered antagonistic; if it is less than the lower OCI, the joint toxic action of the mixture ray is considered synergistic. The toxic effect of the mixture is considered additive when the combined toxicity calculated by the IA model is between the two OCIs.

Biochemical Index Determination

The reactive oxygen species (ROS) activity was determined using a fluorescence spectrophotometer (LS55, PerkinElmer, USA) according to a previous report [25]. The superoxide dismutase (SOD) activity was determined using an SOD assay kit (A001-2, Nanjing JianCheng Bioengineering Institute, Nanjing, China) in accordance with the manufacturer's instructions. The absorbance was obtained at 450 nm using a UV-vis spectrophotometer (T3200, Yoke, China). Relative SOD levels were calculated as the ratio of the treatment group to the control group.

Altered algal cell permeability was determined using a fluorescence spectrophotometer in accordance with a previous report [25] using fluorescein diacetate (FDA) as a coloring agent. The mitochondrial membrane potential loss was measured by fluorescence

Table 2. Mixture ratios ($p_{i,j}$) of the two components (j = 1, 2) in the six mixture rays (i = 1, 2, 3).

No	Mixture ray	$p_{i,j}$ (i = 1, 2, 3; j = 1, 2) (%)		
		GO	C-SWCNT	GOQD
1	GO-C-SWCNT-R1	50.5	49.5	
2	GO-C-SWCNT-R2	75.4	24.6	
3	GO-C-SWCNT-R3	90.2	9.8	
4	GO-GOQD-R1	33.4		66.6
5	GO-GOQD-R2	50.0		50.0
6	GO-GOQD-R3	66.6		33.4

microscopy (IX71, Olympus, Japan) and recorded as the ratio of the red-to-green emission intensities (I590/I530) in accordance with a previous report [25].

Metabolic Analyses

The algal suspension was centrifuged (9000 g, 5 min), freeze-dried, and ground to a uniform powder. The algal cell powder was stored at −80ºC until metabolic analysis. For the metabolic analysis, a 4.5 mL solution of methanol and water (4:1 volumetric ratio) was used to resuspend the cell powder sample, and the cells were completely broken by three freeze-thaw cycles in liquid nitrogen. To extract the metabolites, the samples were ultrasonicated (200 W, 30 min), vortexed (4 min), and then centrifuged at 18,730 *g* for 10 min at 4ºC. This extraction procedure was repeated twice for each cell pellet, and the supernatants of the two extraction rounds were mixed. Next, 500 µL of supernatant was freeze-dried in a vacuum concentrator for 24 h. Methoxamine hydrochloride (20 mg/mL, 50 µL) and N-methyl-N-(trimethylsilyl) trifluoroacetamide (80 µL) were added to the dried samples for derivatization. The sample supernatant (150 µL) was then transferred to a glass injection vial for gas chromatography-mass spectrometry (GC-MS) analysis. A Shimadzu single quadrupole GC-MS QP2010 (Kyoto, Japan) was used for the analysis.

Statistical Analysis

All of the experiments were performed in triplicate, and the results are presented as the mean±standard deviation. To analyze differences between the exposed groups and the control, significant differences were determined by one-way analysis of variance (ANOVA) using the least significant difference, followed by Duncan's test in heat map. In the pathway analysis, significant differences were determined by two-way analysis of variance (ANOVA), which was used to achieve the discrimination of two independent factors using MetaboAnalyst 5.0 (http://www.metaboanalyst.ca/). Statistical significance was accepted at $p<0.05$. A heat map was generated using Multiple Experiment Viewer (version 4.9.0, Dana-Farber Cancer Institute, Boston, MA, USA) to depict relationships between the significantly differential metabolites among the samples. Visualization and Analysis of NeTworks Containing Experimental Data (VANTED, version 2.1.0) was used to create the pathway map.

Results

Toxicities of Individual Nanomaterials in *M. aeruginosa*

Fig. 1 shows plots of *M. aeruginosa* inhibition vs. the logarithm of the individual nanomaterial concentrations on the third and seventh days. GO and C-SWCNT had significant inhibitory effects but were less than 60% on the third day and less than 40% on the seventh day. The J-shaped concentration-response effect of GOQD indicated a significant hormetic effect over a wide concentration range. The CRCs were well fitted. The equation model, statistics (R and RMSE), and hormetic effect ranges are presented in Table 3. The R values were >0.9049, indicating good relationships between the nanomaterial exposure concentrations and *M. aeruginosa* inhibition.

As shown in Fig. 1, GOQD was much more toxic than either GO or C-SWCNT in the low- and high-dose ranges, but it was less toxic in the medium-dose range because of the hormetic effect on the third day. GOQD toxicity on the third day was lower than on the seventh day, while the hormetic effect was much higher on the seventh day. Maximum stimulation was 44% on the third day but 104% on the seventh day. The GO and C-SWCNT inhibition rates on the third day were higher than on the seventh day.

As shown in Fig. 2a) and b), 0.01-10 mg/L GOQD significantly promoted the ROS and SOD levels, which were significantly higher than those in the GO- and C-SWCNT-treated groups. The relative ROS and SOD

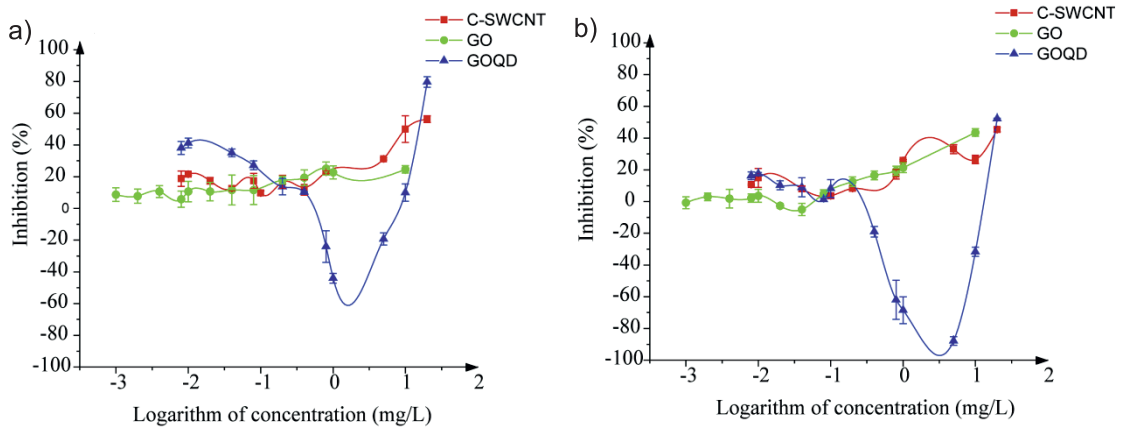

Fig. 1. Toxic effects of GO, C-SWCNT, and GOQD on the third a) and seventh day b).

Table 3. CRC models of individual and binary nanomaterial mixtures on the seventh day.

Nanomaterials		Equation model	R	RMSE	Hormetic effect	Maximum stimulation (%)
Single	GO	Sine	0.9704	3.220	No	
	SWCNT	Lorentz	0.9049	5.603	No	
	GOQD	BoltzIV	0.9922	5.221	Yes	104.0
Binary mixture	GO-C-SWCNT-R1	Sine	0.9996	0.219	Yes	12.35
	GO-C-SWCNT-R2	Gauss	0.9764	1.334	No	
	GO-C-SWCNT-R3	Gauss	0.9734	1.251	No	
	GO-GOQD-R1	BoltzIV	0.9696	10.722	Yes	87.34
	GO-GOQD-R2	BoltzIV	0.9971	3.209	Yes	84.40
	GO-GOQD-R3	Rational5	0.9941	4.708	Yes	97.47

levels were 113-115% in the GO group and 119%-120% in the C-SWCNT group at the low nanomaterial concentrations of 0.01, 0.1, and 1 mg/L. These values were only slightly higher than those of the control group. In contrast, at 10 mg/L, the ROS and SOD levels of C-SWCNT were 135% and 185%, respectively, and were significantly higher than in the control. The cell permeability and mitochondrial membrane potential loss results are shown in Fig. 2c) and d). The permeability of algae cells exposed to C-SWCNT was significantly higher than of those exposed to either GO or GOQD. No significant differences between the nanoparticle-exposed groups and the control were found at the low exposure concentration. Compared with the control, the red-to-green fluorescence intensity ratios were significantly decreased by 90.28% ($p<0.05$)

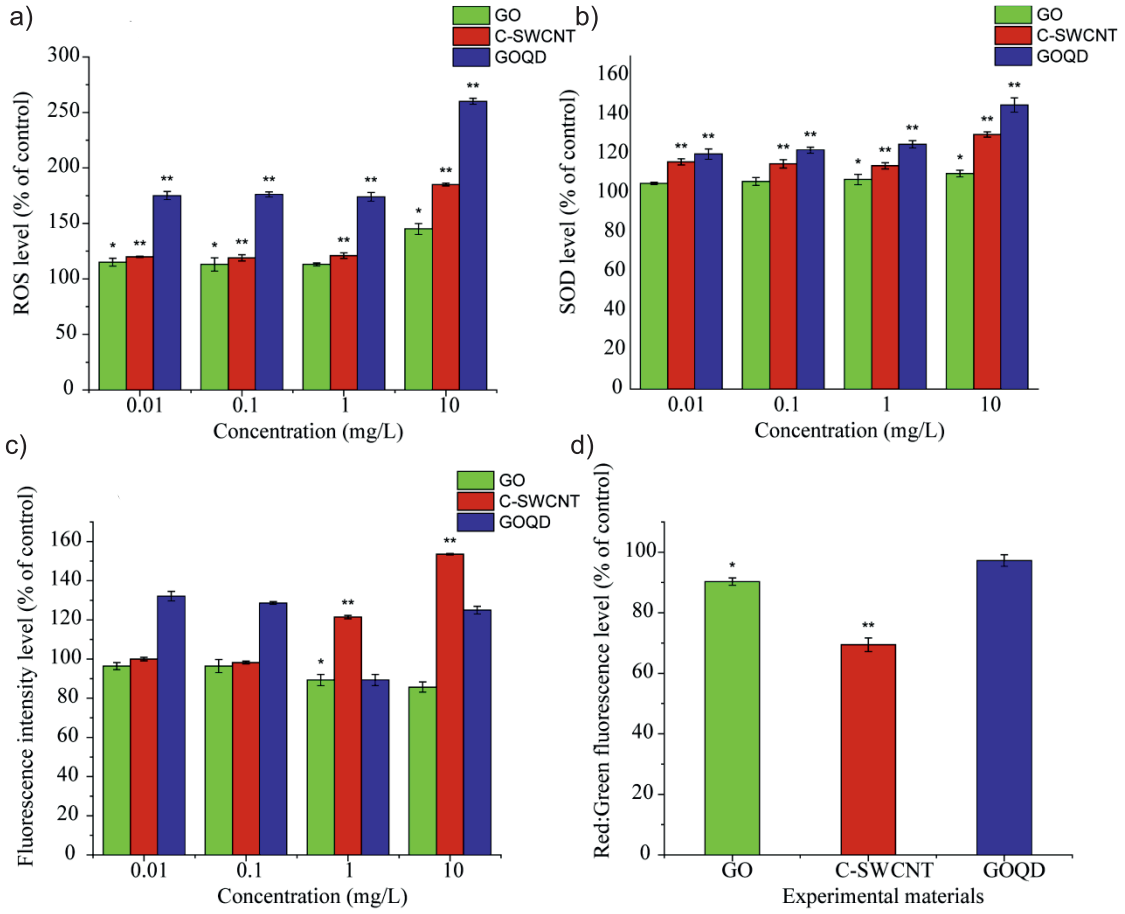

Fig. 2. Alterations in the ROS levels a), SOD activities b), cell permeability c), and mitochondrial membrane potential loss d) after exposure to nanomaterials for 72 h (3 d). *$p<0.05$, **$p<0.005$ compared with control.

and 69.44% ($p<0.005$) after exposure to 1 mg/L GO and C-SWCNT, respectively. There was no significant difference between the GOQD group and the control.

Toxicities of the Binary Mixtures

Fig. 3 shows the CRCs of *M. aeruginosa* exposed to the six nanomaterial rays (GO-C-SWCNT-R1, GO-C-SWCNT-R2, GO-C-SWCNT-R3, GO-GOQD-R1, GO-GOQD-R2, and GO-GOQD-R3). The CRC of each binary mixture was well fitted. The statistics (R and RMSE) and hormetic effect ranges are presented in Table 3.

The toxic effect of the GO-C-SWCNT mixture was stronger on the third day than on the seventh day, especially at the low and high concentrations (Fig. 3a and b). The joint effect of GO and C-SWCNT (R1) showed greater toxicity than any of the other rays. The combined toxicity increased as the GO proportion in the binary mixture increased. As shown in Fig. 3a) and c), the CRCs of the GO-GOQD rays are steeper than those of GO-C-SWCNT, and the inhibitory trend of GO-C-SWCNT increases more slowly. The results of the GO-GOQD mixture rays varied with the culture time. On the third day, the toxicities of the GO-GOQD mixtures were similar to that of GO alone, but on the seventh day, this pattern changed and resembled the pattern seen with GOQD alone. That is, the hormetic effect of the GO-GOQD rays on the seventh day was much stronger than on the third day. The hormetic effect of GO-GOQD-R3 was much stronger than that of the other GO-GOQD rays (Table 3). The maximum hormetic effect of GO-GOQD-R3 based on the fitting function was 104.0%. However, increasing the GOQD proportion in the binary mixture did not result in a stronger hormetic effect.

The combined toxicity of a mixture can be assessed by comparing the IA curve with the actual dose–response curve of the mixture and its corresponding OCI limits. The fitted CRCs, OCIs, and IA models are shown in Fig. 4. For GO-C-SWCNT-R1 and GO-C-SWCNT-R2, the predicted inhibitions were greater than the upper OCI, indicating that the joint toxic actions of these mixture rays exhibited antagonism. In GO-C-SWCNT-R3, only one low concentration in the prediction model was located below the lower OCI, indicating synergism. Another low concentration was located between the OCIs, while the remaining six predicted inhibitions were all greater than the upper OCI, indicating that the combined toxicity exhibited both additive effects and antagonistic, respectively. The three GO-GOQD mixture rays had the same overall trend. Antagonism occurred at low and middle concentrations, but additive and synergistic toxicity occurred at high concentrations.

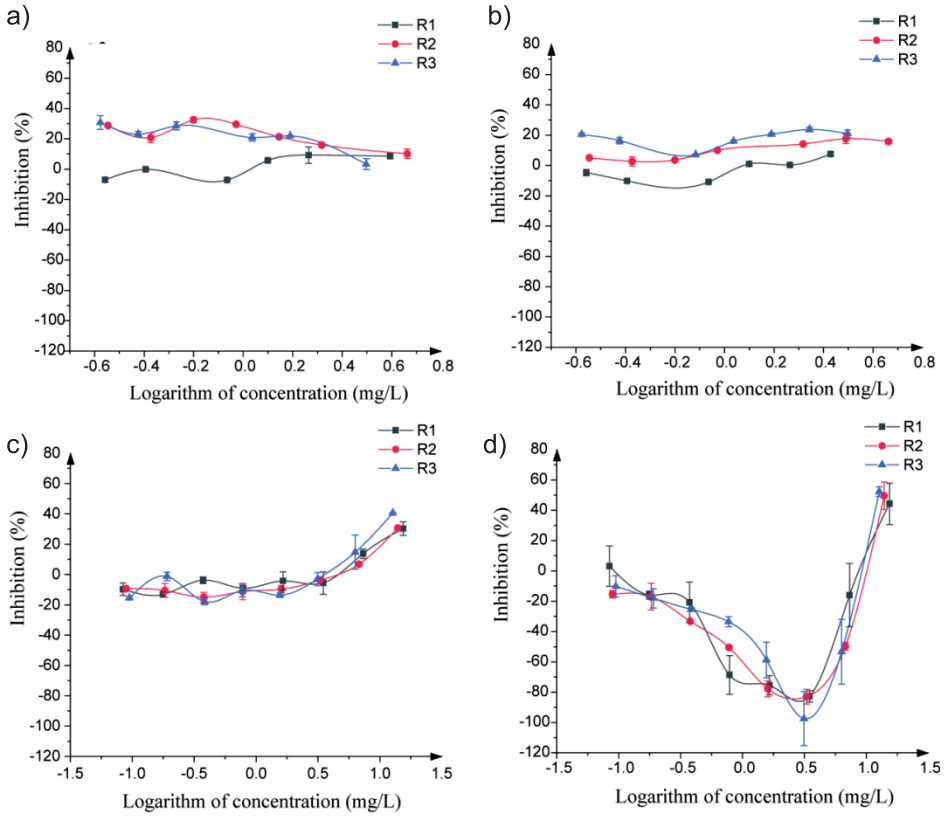

Fig. 3. Toxic effect of the binary mixture rays. GO-C-SWCNT on the third day a); GO-C-SWCNT on the seventh day b); GO-GOQD on the third day c); and GO-GOQD on the seventh day d). Six rays (denoted as GO-C-SWCNT-R1, GO-C-SWCNT-R2, GO-C-SWCNT-R3, GO-GOQD-R1, GO-GOQD-R2, and GO-GOQD-R3) of the two components are listed in Table 2.

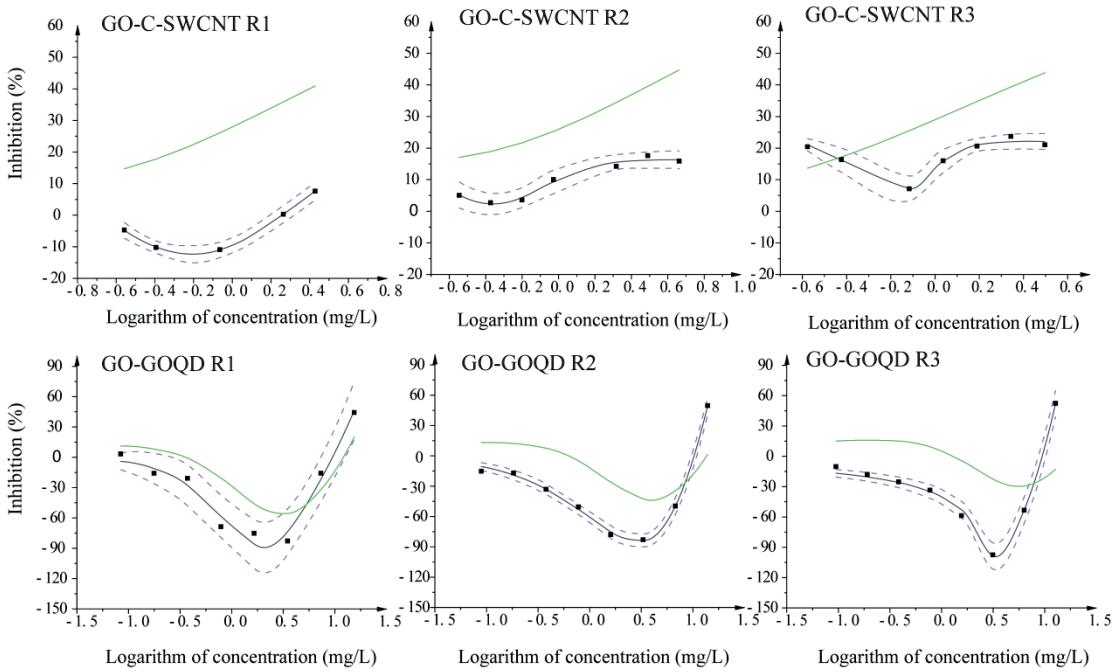

Fig. 4. Concentration–inhibition profiles of the six binary mixtures. Black solid squares indicate the experimentally observed values; black solid lines indicate the fitted CRCs; purple dashed lines indicate the OCIs; and green solid lines indicate the predicted IA models.

Metabolic Analysis

Overall, 66 metabolites were identified by GC-MS; these included amino acids (11), carbohydrates (18), organic acids (15), fatty acids (7), and other small molecule metabolites (15). There were significantly different between the control and nanomaterials treated groups and 54 metabolites were screened by ANOVA with $p<0.5$. A heat map was created to understand the differences in metabolites between the control and the groups exposed to 1 mg/L nanomaterial (Fig. 5). Hierarchical clustering (HCL) was performed with average linkage and Pearson correlation analyses. Using HCL analysis, the samples were divided into two clusters: control&GO and C-SWCNT&GOQD. The metabolites were also divided into two clusters. HCL analysis was used to identify differences in the metabolic profiles among the control, GO, C-SWCNT, and GOQD groups. Compared with the control group, the GOQD and C-SWCNT groups had higher contents of fatty acids and carbohydrates, respectively, which are related to glycolysis, while the GO group had a higher content of the major amino acids. The results of metabolic changes among the control, GO, C-SWCNT, and GOQD groups, followed by HCL, suggested that C-SWCNT and GOQD exerted a stronger influence on the algal metabolic profile than GO did.

The cell cultures exposed to the three nanomaterials at 0.01, 0.1, 1, and 10 mg/L underwent metabolic profiling, and the analysis results are shown in Fig. 6. The profiling revealed strong involvement of sugar metabolism, branched-chain amino acid (BCAA) metabolism, amino acid metabolism, and fatty acid (FA) metabolism. For sugar metabolism (except for glucose), significant differences from the control were observed for all exposure groups, especially at the low concentrations of 0.01 and 0.1 mg/L. The levels of fructose, melibiose, and mannose decreased with increasing C-SWCNT concentration, but they increased with increasing GO and GOQD concentrations. Regarding amino acid metabolism, in the GO group, all detected amino acids decreased with increasing nanomaterial concentration, and these decreases were significantly greater than in the C-SWCNT and GOQD groups. Except for isoleucine, the BCAAs levels in the GOQD group showed greater increases than in any of the other exposure groups, especially at the high exposure concentrations. Regarding FA metabolism, the long-chain FAs had the highest contents in the GOQD group at the 0.1, 1, and 10 mg/L exposure concentrations.

Discussion

The particle size of nanomaterials is an important factor in their biological distribution, absorption, transfer, transformation, and toxicity [4]. The toxicity of nanomaterials is closely related to their physical and chemical properties [26, 27]. The chemical properties of the nanomaterial surface are strongly related to their distribution in solution and their cellular interactions. To examine the nanotoxicology and possible associated mechanisms of action, three typical nanomaterials were chosen as the research object in this study: GO, C-SWCNT, and GOQD.

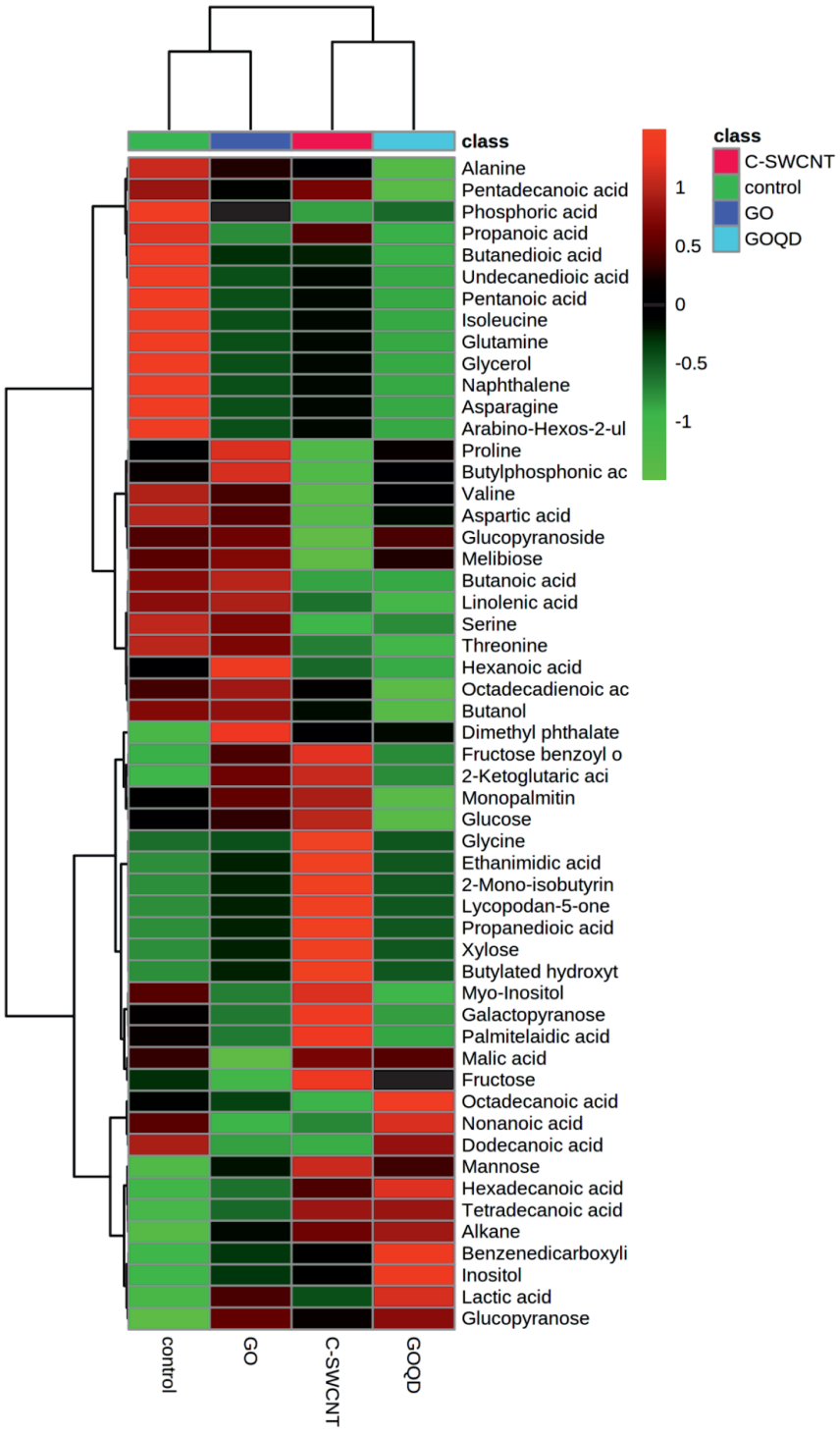

Fig. 5. Heat map of the identified metabolites in the control and nanomaterial-exposed groups. Red and blue indicate the relative metabolite contents: Red indicates higher contents, and blue indicates lower contents. Abbreviations: Graphene oxide (GO), GO quantum dots (GOQD), Carboxylic acid-functionalized single-walled carbon nanotubes (C-SWCNT).

Toxicity Mechanism of Individual Nanomaterials

Oxidative stress, as indicated by the ROS and SOD levels, was investigated 72 h after exposing the cells to 0.01, 0.1, 1, and 10 mg/L nanomaterial (Fig. 2). In the enzymatic system, SOD is the first defense against reactive oxygen species in algae cells. The order of the ROS and SOD levels was GOQD>C-SWCNT>GO. Mitochondria are also important sites for producing oxidative free radicals; therefore, the loss of the mitochondrial membrane potential can change the oxidative stress levels in cells. The stronger the red-to-green fluorescence ratio, the healthier the mitochondria.

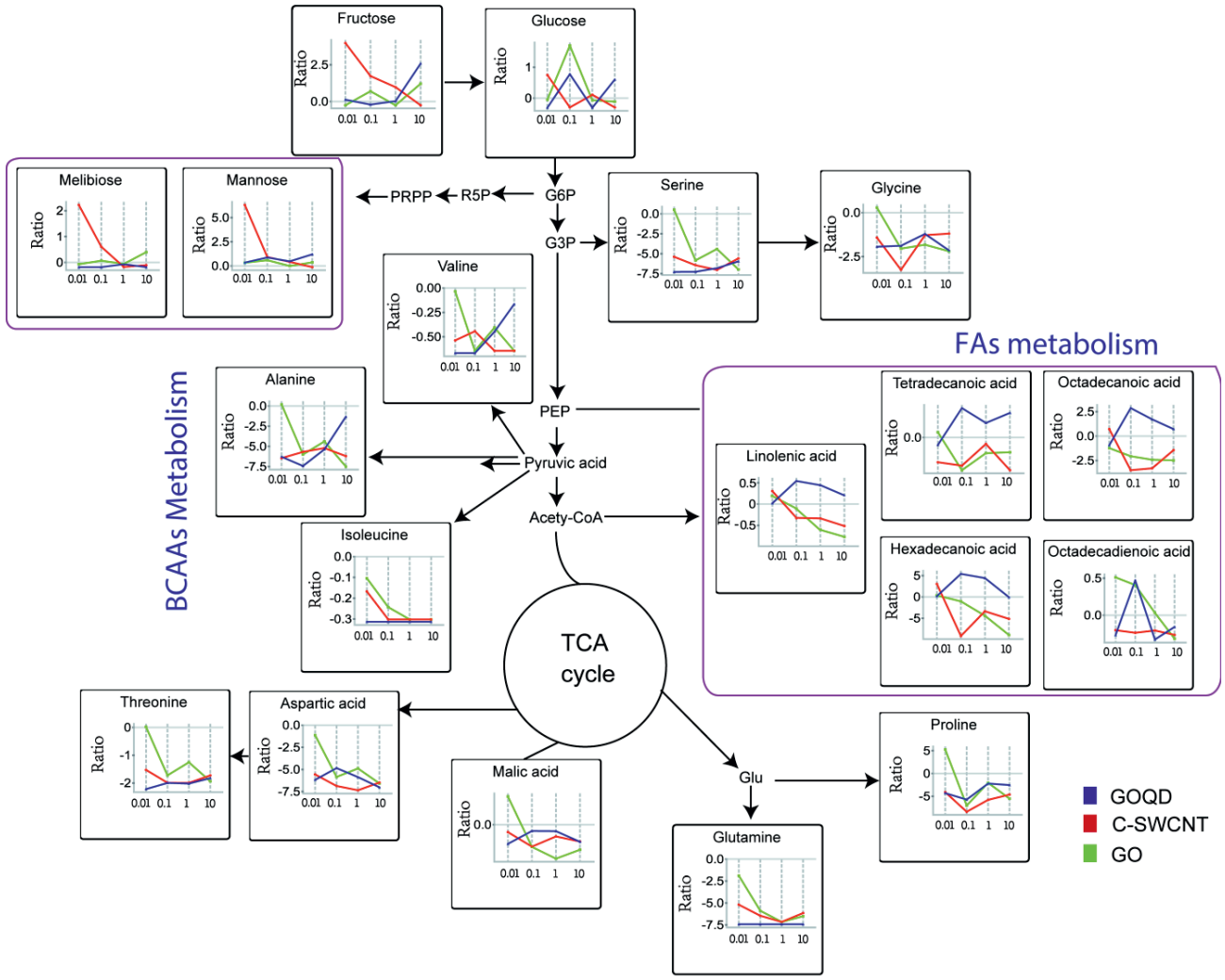

Fig. 6. Pathway map of the differentially expressed metabolites involved in sugar, amino acid, fatty acid, and glycolysis metabolism. Red line indicates carboxylic acid-functionalized single-walled carbon nanotubes (C-SWCNT), blue line indicates GO quantum dots (GOQD), and green line indicates graphene oxide (GO). Significant metabolites involved in the pathway were screened by two-way analysis of variance (ANOVA) at $p < 0.0001$. Metabolic profiling was conducted after exposing the cells to 0.01, 0.1, 1, and 10 mg/L nanomaterial for 72 h. The ratio of nanomaterials treated groups to control groups for each metabolite was subjected to pathway analysis.

This ratio was the highest in the GOQD group and was not significantly different from the control, indicating that the algae cells exposed to GOQD were healthier than the other exposure groups. The cell permeability is indicated by the FDA fluorescence intensity, where a stronger intensity indicates lower cell permeability and thus greater membrane integrity. The cell permeability is closely related to oxidative stress. Although the ROS and SOD levels were the highest in the GOQD group, the FDA fluorescence intensity at high exposure concentrations was low because of the hormetic effect, especially at 1 mg/L.

The hormetic effect is related to the elimination of free radicals (via oxidation and antioxidation). In the body, when cells are stimulated by the external environment to produce ROS, the activity of antioxidant enzymes rapidly increases to eliminate the ROS, thereby protecting the body. The low concentrations of nanomaterials activated the oxidation system of the algae cells but did not produce oxidative stress. The hormetic effect might reduce the ROS content in algae cells, thereby promoting algal cell growth. The hormetic effect in the GOQD-treated group induced a marked rise in ROS and SOD as the GOQD concentration increased, indicating that the oxidation system was stimulated. However, the relatively low level of FDA fluorescence intensity and high red-to-green fluorescence ratio implied that the hormetic effect induced by 1 and 10 mg/L GOQD did not produce oxidative stress, and these cells had little cell permeability and healthy mitochondria. The results confirmed that the hormetic effect helped to maintain high algae cell growth rates while successfully managing macromolecular damage. Oxidative stress was induced by GO and C-SWCNT, which damaged the cells and inhibited the proliferation of *M. aeruginosa*.

Altering the mitochondrial membrane potential and inducing oxidative stress are considered to be the main mechanisms of nanotoxicology, but these nanotoxicological mechanisms have not been further elaborated by assessing the metabolic pathways of small molecules in cells. To clarify the nanotoxicology mechanisms, metabolic profiling was conducted after exposing the cells to 0.01, 0.1, 1, and 10 mg/L nanomaterial for 72 h (Fig. 6). The ratio of nanomaterials treated groups to control groups for each metabolite was subjected to pathway analysis. The three nanomaterials investigated exhibited different dose-response relationships with *M. aeruginosa*. The CRCs of GO and C-SWCNT showed no hormetic effect (Fig. 1). GO caused mild growth inhibition at all concentrations. The growth inhibition caused by GO increased slightly with culture time. There was no significant increase in inhibition by exposure to C-SWCNT, but the toxicity of C-SWCNT was higher than that of GO. The CRCs of the GOQD group were J-shaped, indicating a significant hormetic effect; furthermore, with the prolongation of culture time, the maximum stimulation and hormetic effect range were increased, but the toxicity was decreased. GOQD caused strong inhibition only at the high concentration. These results suggest that GO, C-SWCNT, and GOQD have different toxic mechanisms in *M. aeruginosa*, which was confirmed by the metabolic analysis.

Sugars are the products of photosynthesis and strongly influence cell wall synthesis [28]. In response to C-SWCNT toxicity, the sugar content decreased significantly, which was thought to be caused by the consumption of sugars. The inherent characteristics of amino acids enable them to promote energy metabolism and photosynthesis [29]. In particular, glycine and serine can increase the chlorophyll content of plants, improve enzyme activity, promote the penetration of carbon dioxide, and make photosynthesis more vigorous. Amino acid depletion was the most obvious in the GO-treated group, with declines in glycine, serine, threonine, aspartic acid, and glutamine; however, the BCAAs were not depleted. The BCAA levels in the GOQD group increased with the exposure concentration, which might have resulted from the hormetic effect. The hormetic effect stimulated the growth of algae cells, which induced protein synthesis. BCAAs are important components in protein synthesis. Moreover, the biosynthesis of unsaturated fatty acids is related to cell permeability and plasmolysis [30]. As a membrane lipid, linolenic acid contributes to membrane fluidity, and changes in this unsaturated fatty acid induce perturbations in the plasma membrane. Therefore, linolenic acid upregulation in the 0.1, 1, and 10 mg/L exposure groups was induced by the hormetic effect. This is consistent with the fact that GOQD likely reduced the loss of mitochondrial membrane potential and triggered the oxidation system but did not affect oxidative stress (Fig. 2a).

Previous reports have found that *M. aeruginosa* cells have a diameter of approximately 5 μm, which is similar to the size of GO [25]. GO was found to cover the surface of the cells, causing a shielding effect. Both C-SWCNT and GOQD could be internalized by the cells [25, 31]. The cellular uptake of C-SWCNT occurred more readily than GO owing to its smaller size. GOQD was the smallest of the investigated nanomaterials and showed the largest uptake because it could permeate the cell wall and be endocytosed. Based on the metabolic perturbations, nanomaterial exposure led to a resource reallocation among photosynthesis, cell wall synthesis, and energy metabolism. The metabolic analysis showed that the nanomaterials induced different resource reallocations, which was indicated by the sugar, amino acid, and FA contents. There are several possible reasons for this phenomenon. First, the shielding effect of GO might have inhibited photosynthesis and energy metabolism, resulting in sharp declines in amino acids. Second, C-SWCNT may have permeated the cell wall during internalization, thus fracturing the cell wall. This would induce cell wall synthesis pathways, indicated by the melibiose and mannose contents. Third, the synergistic effect of hormesis and internalization may have led to the promotion of fatty acid metabolism and then inhibition in the GOQD-treated group. Our findings suggest that metabolic analysis is potentially useful in the ecological risk assessment of nanomaterials.

Joint Action Prediction by the IA Models

In the GO-C-SWCNT-R1 and GO-C-SWCNT-R2 mixture systems, the two rays exhibited antagonism over the entire concentration range (Fig. 4). GO produces a shielding effect, whereas C-SWCNT is internalized, and the combined effect inhibited cell proliferation. However, because the shielding effect of GO hindered C-SWCNT internalization, the joint toxic action was antagonistic. The low concentration of the GO-C-SWCNT-R3 mixture produced a joint synergistic action, and it can be inferred that it resulted in a combined effect on proliferation.

The toxicological interactions between GO and GOQD differed according to their respective concentrations, with antagonism at low doses and synergism at high doses. The mechanisms for the joint actions might vary because of differences in the individual toxic mechanisms of GO and GOQD. Middle concentrations of GOQD significantly increased the cell growth rates because of the hormetic effect, while GO significantly decreased the cell growth rates owing to internalization. The opposing effects of promoting and inhibiting cell growth produced by GOQD and GO may have weakened their combined toxicity in *M. aeruginosa*. Therefore, the joint toxic action of the GOQD and GO mixture is antagonistic. With increasing GOQD concentration, there was a shift from the hormetic effect to internalization; as

a result of GOQD and GO internalization, the high-concentration mixtures exhibited a joint synergistic action.

Understanding the reasons underlying the toxicity of mixtures of common nanomaterials that often coexist will help us to understand the toxicity mechanisms of other similar combinations, ultimately improving the accuracy of risk assessment. Our findings indicate that such mixtures may even produce stimulatory effects in *M. aeruginosa*. Notably, the hormetic effect in *M. aeruginosa* and its possible contribution to algae blooms may increase the harm of nanomaterials. Freshwater cyanobacteria blooms usually comprise competitive nontoxic and toxic species and strains [4, 32]. The hormetic effects of nanomaterials in *M. aeruginosa* may profoundly impact the dynamic changes in the abundance and proportions of nontoxic and toxic species, which would determine the algal bloom toxicity and could influence the formation and trends of cyanobacteria blooms. Hence, there is an urgent need to include hormesis in environmental risk assessments of pollutants.

Conclusion

This study investigated the toxicity of single and binary nanomaterials, namely, GO, C-SWCNT, and GOQD, in *M. aeruginosa*. A hormetic effect on proliferation was observed for GOQD and for the GO–GOQD mixtures, with maximum stimulation ranging from 84.40% to 104.0%. The toxicological mechanisms of these nanomaterials were analyzed through metabolic profiling. Regarding the metabolic status of the algae exposed to the three nanomaterials, the sugar contents were significantly downregulated in the C-SWCNT-treated group, amino acid depletion was strongest in the GO-treated group, and the FA levels in the GOQD-treated group were higher than in the other treatment groups. These metabolic variations indicated that distinct toxic mechanisms were induced by different metabolic pathways. We propose that these metabolites could be used as indicators of the corresponding biological toxicity of nanomaterials. The experimental results indicate that the overall joint antagonistic action of the GO-C-SWCNT mixtures derives from the shielding of GO interfering with C-SWCNT internalization. The joint toxic action of the GO-GOQD mixture shifted from antagonism to synergism. This change occurred because of a shift from antagonism between shielding and the hormetic effect to cooperation between shielding and internalization. This study provides toxicity data and mechanisms for three nanomaterials and demonstrates the complexity of the individual and joint toxic actions. The findings will benefit the growing field of nanomaterial toxicological research. The striking hormetic effect of nanomaterials in *M. aeruginosa* may aggravate the harm of these materials because of their potential ability to amplify algae blooms. Therefore, the hormesis effect should be included in pollutant risk assessments.

Acknowledgments

This research was sponsored by the Key Research and Development Program of Hebei Province under Grant 20373902D, the Scientific Research Key Projects of Education Department of Hebei Province ZD2021038, The three three three talent engineering personnel training funding C20221034, Hebei Province Education Department Outstanding Youth Program BJK2022058, Hebei Province Education Department Outstanding Youth Program BJ2021049. We thank Katherine Thieltges from Liwen Bianji (Edanz) (www.liwenbianji.cn/) for editing the English text of a draft of this manuscript.

Conflict of Interest

The authors declare no conflict of interest.

References

1. LI F., JIANG X., ZHAO J., ZHANG S. Graphene oxide: A promising nanomaterial for energy and environmental applications. Nano Energy **16**, 488, **2015**.
2. PRIYADARSINI S., MOHANTY S., MUKHERJEE S., BASU S., MISHRA M. Graphene and graphene oxide as nanomaterials for medicine and biology application. J. Nanostructure Chem. **8**, 123, **2018**.
3. DREYER D.R., PARK S., BIELAWSKI C.W., RUOFF R.S. The chemistry of graphene oxide. Chem. Soc. Rev. **39**, 228, **2010**.
4. SEABRA A.B., PAULA, A.J., de LIMA R., ALVES O.L., DURÁN N. Nanotoxicity of Graphene and Graphene Oxide. Chem. Res. Toxicol. **27**, 159, **2014**.
5. ALTENBURGER R., WALTER H., GROTE M. What contributes to the combined effect of a complex mixture? Environ. Sci. Technol. **38**, 6353e6362, **2004**.
6. FAUST M., ALTENBURGER R., BACKHAUS T., BLANCK H., BOEDEKER W., GRAMATICA P., HAMER V., SCHOLZE M., VIGHI M., GRIMME L.H. Predicting the joint algal toxicity of multi-component striazine mixtures at low-effect concentrations of individual toxicants. Aquat. Toxicol. **56**, 13e32, **2001**.
7. WANG Z.J., ZHENG Q.F., LIU S.S., HUANG P., Ding, T.T., XU Y.Q. New methods of top-to-down mixture toxicity prediction: A case study of eliminating of the effects of cosolvent from binary mixtures. Chemosphere **289**, 133190, **2022**.
8. ZHANG Y., GAO Q., LIU S.S., TANG L., LI X.G., SUN H. Hormetic dose-response of halogenated organic pollutants on Microcystis aeruginosa: Joint toxic action and mechanism. Sci. Total Environ. **829**, 154581, **2022**.
9. SHAHMOHAMADLOO R.S., POIRIER D.G., ORTIZ ALMIRALL X., BHAVSAR S.P., SIBLEY P.K. Assessing the toxicity of cell-bound microcystins on freshwater pelagic and benthic invertebrates. Ecotoxicol. Environ. Saf. **188**, 109945, **2020**.

10. SHAHMOHAMADLOO R.S., OTIZ ALMIRALL X., SIMMONS D. B. D., LUMSDEN J.S., BHAVSAR S.P., WATSON-LEUNG T., EYKEN A.V., HANKINS G., HUBBS K., KONOPELKO P., SARNACKI M., STRONG D., SIBLEY P.K. Cyanotoxins within and Outside of Microcystis aeruginosa Cause Adverse Effects in Rainbow Trout (Oncorhynchus mykiss). Environ. Sci. Technol. **55**, 10422, **2021**.
11. CRUCES E., BARRIOS A.C, CAHUE Y.P, JANUSZEWSKI B., GIBERTSON L.M., PERREAULT F. Similar toxicity mechanisms between graphene oxide and oxidized multi-walled carbon nanotubes in Microcystis aeruginosa. Chemosphere **265**, 129137, **2021**.
12. SEYED ALIAN R., DZIEWIĘCKA M., KĘDZIORSKI A., KĘDZIORSKI Ł., AUGUSTYNIAK M. Do nanoparticles cause hormesis? Early physiological compensatory response in house crickets to a dietary admixture of GO, Ag, and GOAg composite. Sci. Total Environ. **788**, 147801, **2021**.
13. SUN H., CALABRESE E.J., ZHENG M., WANG D., PAN Y., LIN Z., LIU Y. A swinging seesaw as a novel model mechanism for time-dependent hormesis under dose-dependent stimulatory and inhibitory effects: A case study on the toxicity of antibacterial chemicals to Aliivibrio fischeri. Chemosphere **205**, 15, **2018**.
14. SUN H., CALABRESE E.J., LIN Z., LIAN B., ZHANG X. Similarities between the Yin/Yang Doctrine and Hormesis in Toxicology and Pharmacology. Trends Pharmacol. Sci. **41**, 544, **2020**.
15. MATHIEU A., FLEURIER S., FRÉNOY A., DAIROU J., BREDECHE M.F., SANCHEZ-VIZUETE P., SONG X., MATIC I. Discovery and Function of a General Core Hormetic Stress Response in E. coli Induced by Sublethal Concentrations of Antibiotics. Cell Rep. **17**, 46, **2016**.
16. Agathokleous E., BARCELÓ D., RINKLEBE J., SONNE C., CALABRESE E.J, KOIKE T. Hormesis induced by silver iodide, hydrocarbons, microplastics, pesticides, and pharmaceuticals: Implications for agroforestry ecosystems health. Sci. Total Environ. **820**, 153116, **2022**.
17. VIANT M.R., EBBELS T.M.D., BEGER R.D., EKMAN D.R., EPPS D.J.T., KAMP H., LEONARDS P.E.G., LOIZOU G.D., MACRAE J.I., van RAVENZWAAY B., ROCCA-SERRA P., SALEK R.M., WALK T., WEBER R.J.M. Use cases, best practice and reporting standards for metabolomics in regulatory toxicology. Nat. Commun. **10**, 3041, **2019**.
18. QIU W., LIU X., YANG F., LI R., XIONG Y., FU C., LI G., LIU S., ZHENG C. Single and joint toxic effects of four antibiotics on some metabolic pathways of zebrafish (Danio rerio) larvae. Sci. Total Environ. **716**, 137062, **2020**.
19. ZHAO J., ZHAO Y., HU C., ZHAO C., ZHANG J., LI L. Metabolic Profiling with Gas Chromatography-Mass Spectrometry and Capillary Electrophoresis-Mass Spectrometry Reveals the Carbon-Nitrogen Status of Tobacco Leaves Across Different Planting Areas. J. Proteome Res. **15**, 468, **2016**.
20. ZHAO J., LI L., ZHAO Y., ZHAO C., CHEN X., LIU P. Metabolic changes in primary, secondary, and lipid metabolism in tobacco leaf in response to topping. Anal. Bioanal. Chem. **410**, 839, **2018**.
21. LIU S.S., ZHANG J., ZHANG Y.H., QIN L.T. APTox: assessment and prediction on toxicity of chemical mixtures. Acta. Chim. Sin. **70**, 1511, **2012** [In Chinese].
22. LIU S. S., XIAO Q. F., ZHANG J., YU M. Uniform design ray in the assessment of combined toxicities of multi-component mixtures. Sci. Bull. **61**, 52, **2016**.
23. LIU L., LIU S.S., YU M., CHEN F. Application of the combination index integrated with confidence intervals to study the toxicological interactions of antibiotics and pesticides in Vibrio qinghaiensis sp.-Q67. Environ. Toxicol. Pharmacol. **39**, 447, **2015**.
24. ZHU X.W., LIU S.S., QIN L.T., CHEN F., LIU H.L. Modeling non-monotonic doseresponse relationships: model evaluation and hormetic quantities exploration. Ecotoxicol. Environ. Saf. **89**, 130, **2013**.
25. OUYAN S., HU X., ZHOU Q. Envelopment–Internalization Synergistic Effects and Metabolic Mechanisms of Graphene Oxide on Single-Cell Chlorella vulgaris Are Dependent on the Nanomaterial Particle Size. ACS Appl. Mater. Interfaces **7**, 18104, **2015**.
26. SHARIFI S., BEHZADI S., LAURENT S., LAIRD FORREST M., STROEVE P., MAHMOUDI M. Toxicity of nanomaterials. Chem. Soc. Rev. **41**, 2323, **2012**.
27. SUKHANOVA A., BOZROVA S., SOKOLOV P., BERETOVOY M., KARAULOV A., NABIEV I. Dependence of Nanoparticle Toxicity on Their Physical and Chemical Properties. Nanoscale Res. Lett. **13**, 44, **2018**.
28. VERBANČIČ, J., LUNN J.E., STITT M., PERSSON S. Carbon Supply and the Regulation of Cell Wall Synthesis. Mol. Plant **11**, 75, **2018**.
29. WARREN C.R., DREYER E., ADAMS M.A. Photosynthesis-Rubisco relationships in foliage of Pinus sylvestris in response to nitrogen supply and the proposed role of Rubisco and amino acids as nitrogen stores. Trees **17**, 359, **2003**.
30. YANG H.-B., ZHAO Y.-Z., TANG Y., GONG H.-Q., GUO F., SUN W.-H., CHEN F. Antioxidant defence system is responsible for the toxicological interactions of mixtures: A case study on PFOS and PFOA in Daphnia magna. Sci. Total Environ. **667**, 435, **2019**.
31. HU X., OUYANG S., MU L., AN J., ZHOU Q. Effects of Graphene Oxide and Oxidized Carbon Nanotubes on the Cellular Division, Microstructure, Uptake, Oxidative Stress, and Metabolic Profiles. Environ. Sci. Technol. **49,** 10825, **2015**.
32. LYU K., GUAN H., WU C., WANG X., WILSON A.E., YANG Z. Maternal consumption of non-toxic Microcystis by Daphnia magna induces tolerance to toxic Microcystis in offspring. Freshw. Biol. **61**, 219, **2016**.